# CA9-Targeted Liposomal Delivery of siETS1 Inhibits Clear Cell Renal Cell Carcinoma Progression by Disrupting the ETS1/MYC Regulatory Axis

Yuyang Ye[1], Jing Sun[2], Yizheng Zhang[1], Shenghan Wang[3], Zhaoqian Meng[4, *]

[1]The Second Qilu Hospital of Shandong University, Shandong University, Jinan 250033, P.R.China

[2]Cheeloo College of Medicine, Shandong University, Jinan 250012, P.R.China

[3]Shandong Provincial Hospital Affiliated to Shandong First Medical University, Shandong First Medical University, Jinan 250021, P.R.China

[4]Affiliated Hospital of Shandong University of Traditional Chinese Medicine, Shandong University of Traditional Chinese Medicine, Jinan 250011, P.R.China

* Correspondence

Email: szymzq@163.com

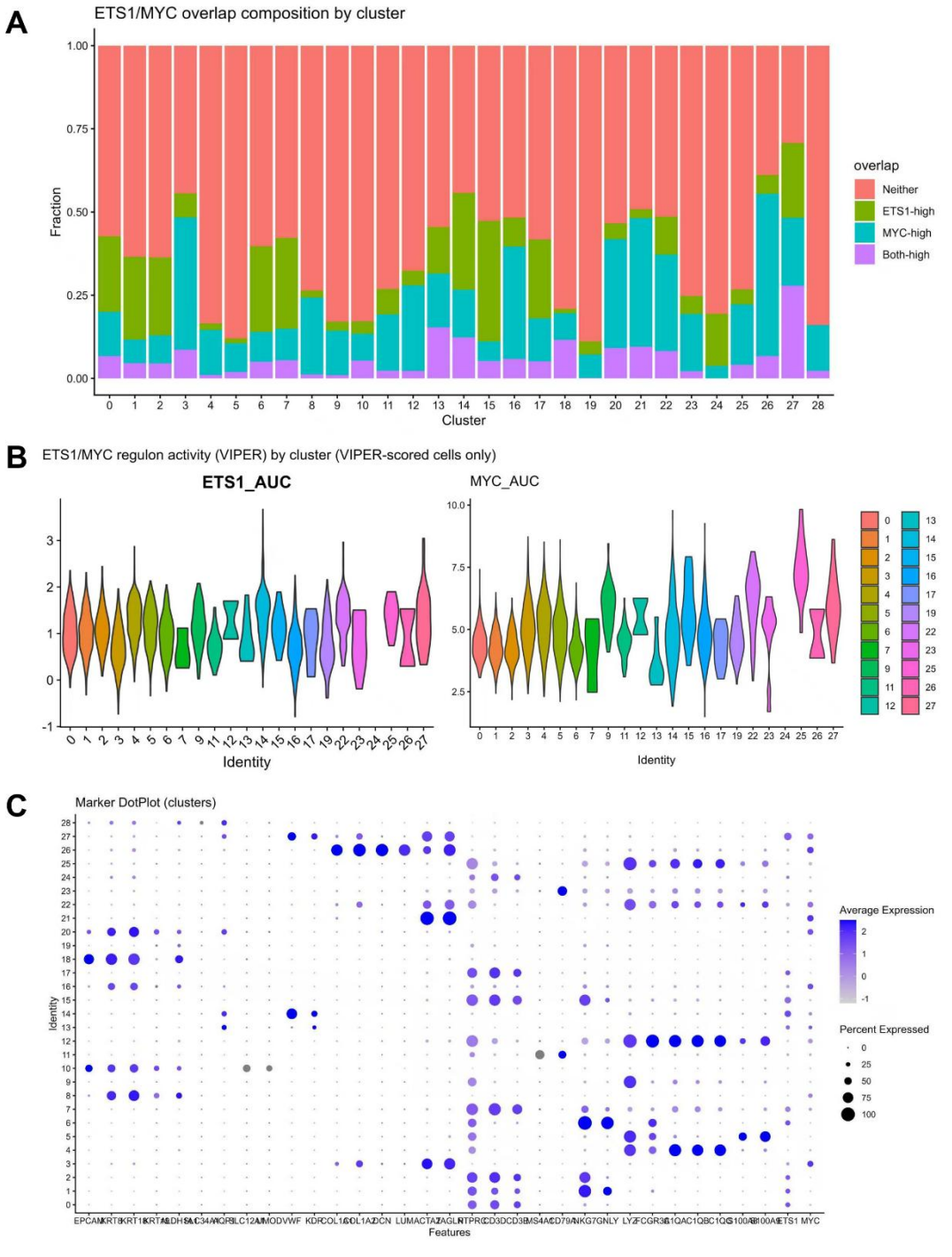


**Supplementary Figure 1. Co-expression and regulon activity analysis of ETS1 and MYC across cell clusters.**

(A) Stacked bar plot illustrating the fraction of cells within each cluster characterized as ETS1-high, MYC-high, or Both-high. (B) Violin plots showing the distribution of ETS1 and MYC regulon activity scores (as inferred by VIPER) across all identified

clusters. (C) Dot plot displaying the expression percentage and average intensity of various marker genes, including ETS1 and MYC, across different cell clusters.

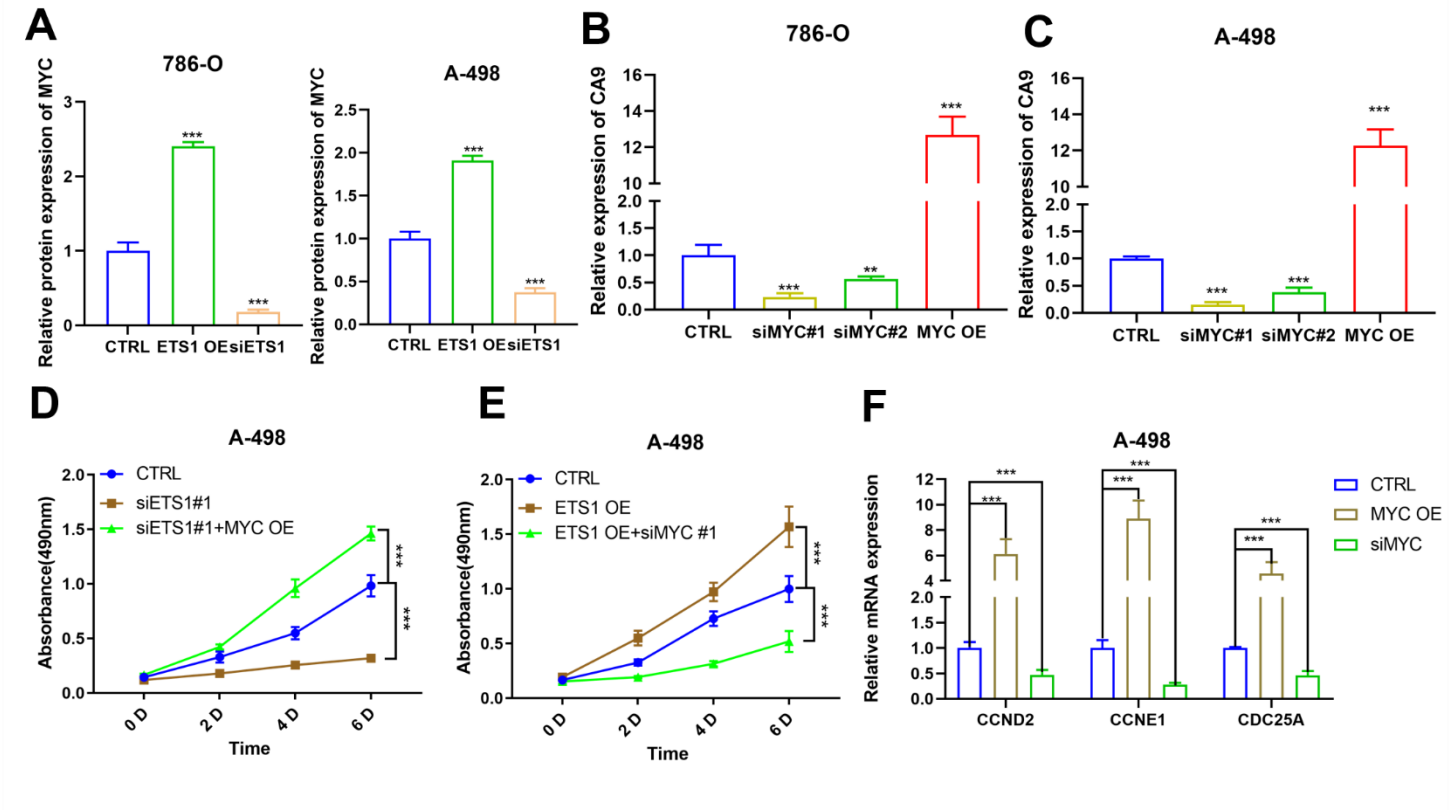


**Supplementary Figure 2 Experimental validation of the ETS1/MYC axis and its impact on the cell cycle**

(A) The protein quantification if MYC in Figure 2F. (B, C) Relative mRNA expression of MYC in 786-O (B) and A-498 (C) cells following treatment with siMYC or MYC overexpression (OE) vectors, confirming transfection efficiency. (D) MTT proliferation curves of A-498 cells showing that MYC overexpression restores growth after ETS1 knockdown. (E) MTT assay demonstrating that silencing MYC inhibits the enhanced proliferation induced by ETS1 OE in A-498 cells. (F) RT-qPCR analysis of the cell cycle markers CCND2, CCNE1, and CDC25A in A-498 cells after modulation of MYC expression in A-498 cells. ** $p < 0.01$, *** $p < 0.001$.

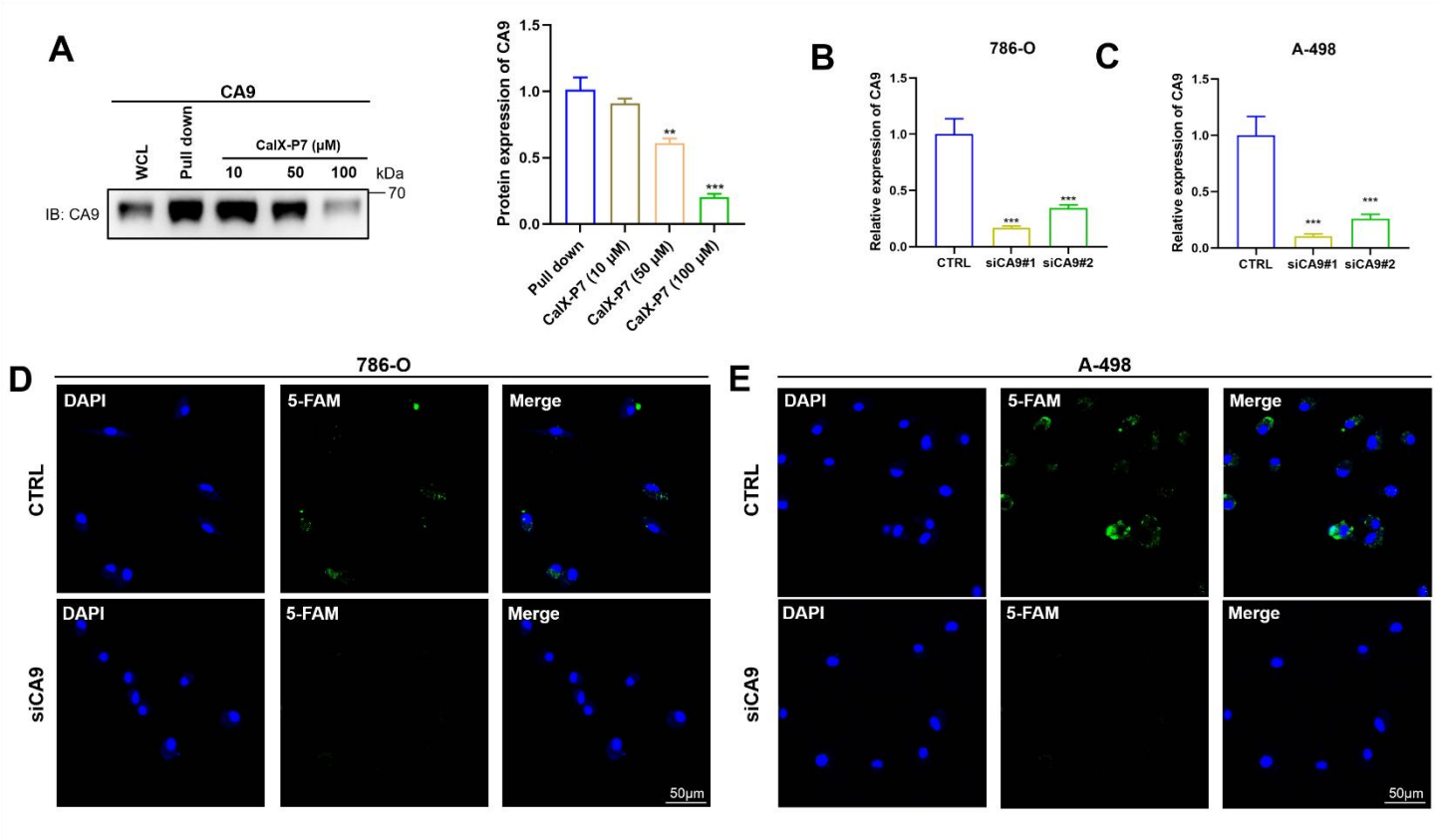


**Supplementary Figure 3 Competitive binding and specificity validation of the optimized peptide CaIX-P7.**

(A) Competitive binding assay using Biotin-conjugated CaIX-P1 and increasing concentrations of CaIX-P7. (B, C) Validation of CA9 knockdown efficiency in 786-O (B) and A-498 (C) ccRCC cell lines following transfection with siCA9 as determined by RT-qPCR. (D, E) Representative fluorescence images showing a significant reduction in the binding and internalization of 5-FAM labeled CaIX-P7 (green) in 786-O (D) and A-498 (E) cells after CA9 silencing. Nuclei were counterstained with DAPI (blue). **: $p < 0.01$; *** $p < 0.001$.

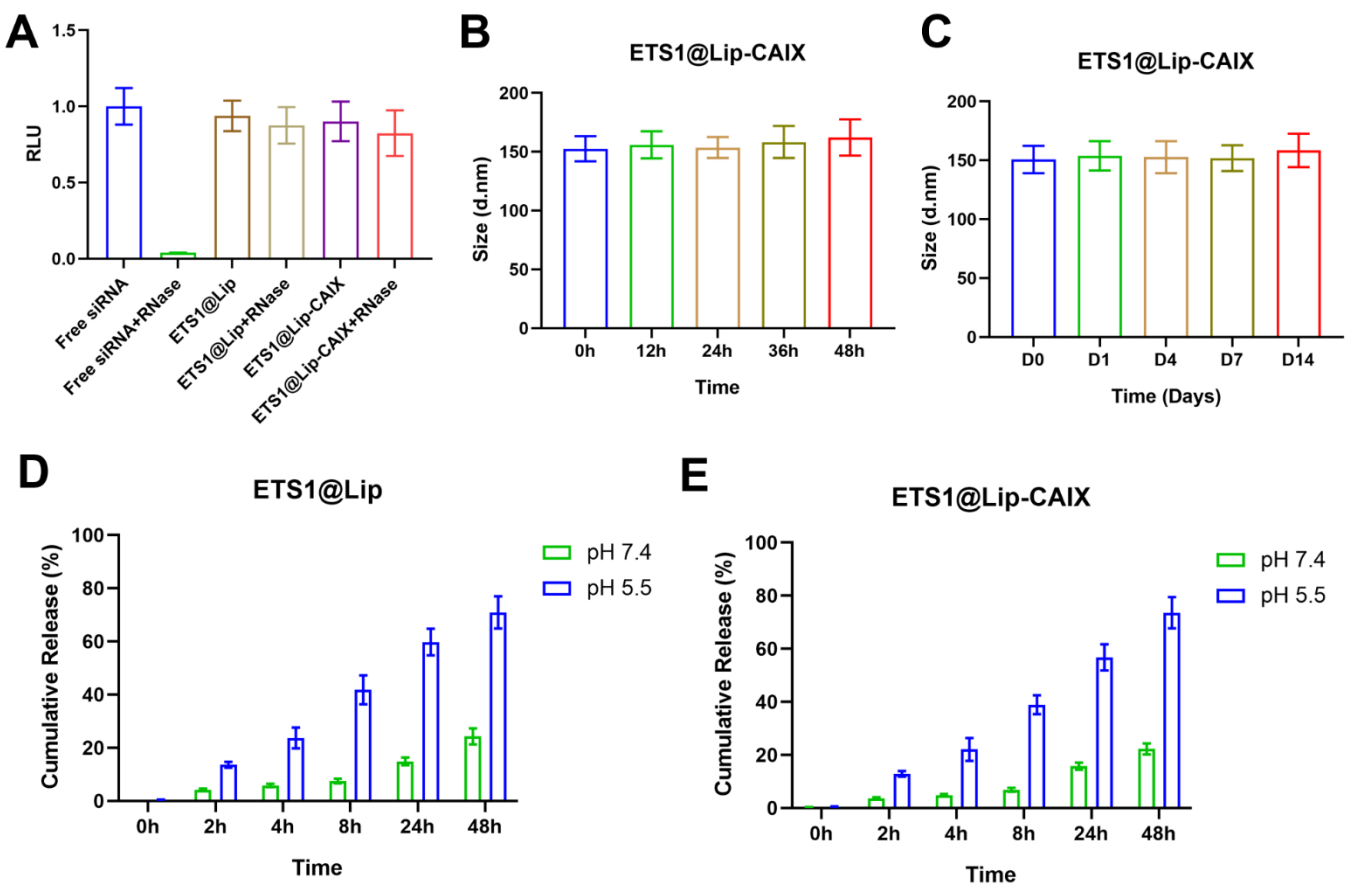


**Supplementary Figure 4 Evaluation of the stability and pH-responsive release of liposomal nanoparticles.**

(A) RiboGreen assay demonstrating the protection of encapsulated siETS1 from RNase degradation. Nanoparticles were treated with RNase, followed by neutralization with EDTA, to assess the integrity of the siRNA cargo compared to free siRNA. (B) Serum stability of ETS1@Lip-CAIX incubated in 10% FBS at 37°C for up to 48 h, as monitored by changes in hydrodynamic diameter via DLS. (C) Long-term storage stability of ETS1@Lip-CAIX in serum at 4°C for up to 14 days. (D, E) In vitro cumulative release profiles of siETS1 from ETS1@Lip (D) and ETS1@Lip-

CAIX (E) at pH 7.4 (simulating physiological conditions) and pH 5.5 (simulating the acidic endo-lysosomal environment). ** $p < 0.01$, *** $p < 0.001$.

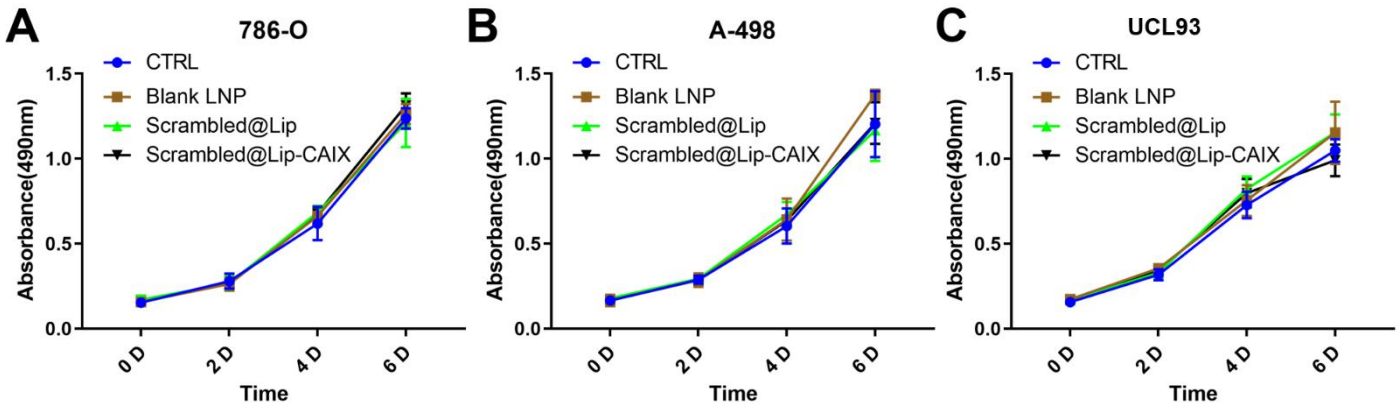


**Supplementary Figure 5 Evaluation of the biocompatibility of the nanocarrier and the specificity of siETS1.**

(A-C) MTT cell proliferation assays showing the growth curves of 786-O (A), A-498 (B), and UCL93 (C) cells treated with empty LNPs (Blank LNP), Scrambled@Lip, or Scrambled@Lip-CAIX.

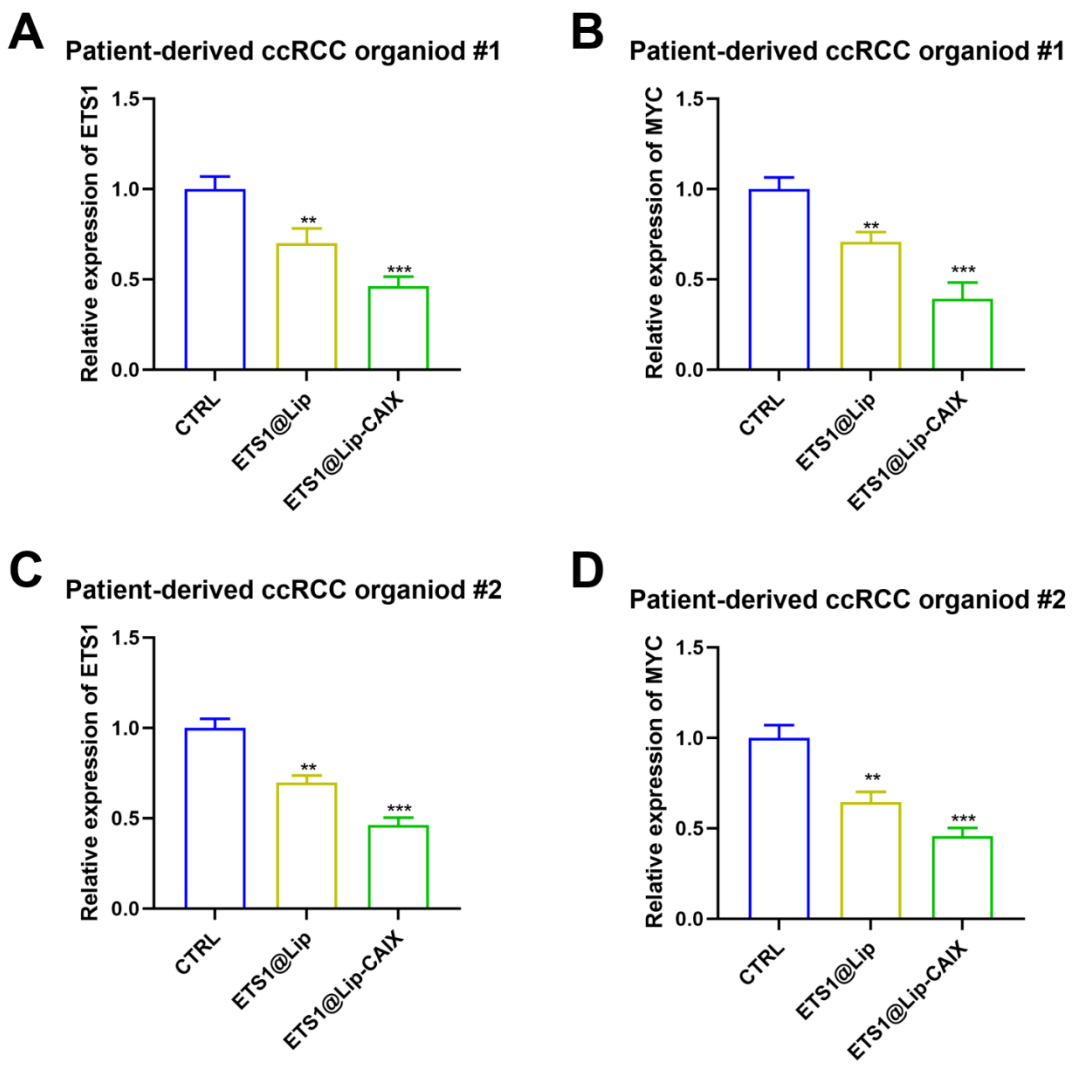


**Supplementary Figure 6 Modulation of ETS1 and MYC expression in patient-derived ccRCC organoids.**

(A, B) Relative mRNA expression levels of ETS1 (A) and MYC (B) in patient-derived ccRCC organoid #1 after treatment with ETS1@Lip or ETS1@Lip-CAIX. (C, D) Relative mRNA expression levels of ETS1 (C) and MYC (D) in patient-derived ccRCC organoid #2 after treatment with the indicated nanoparticles. **: $p<0.01$, ***: $p<0.001$.

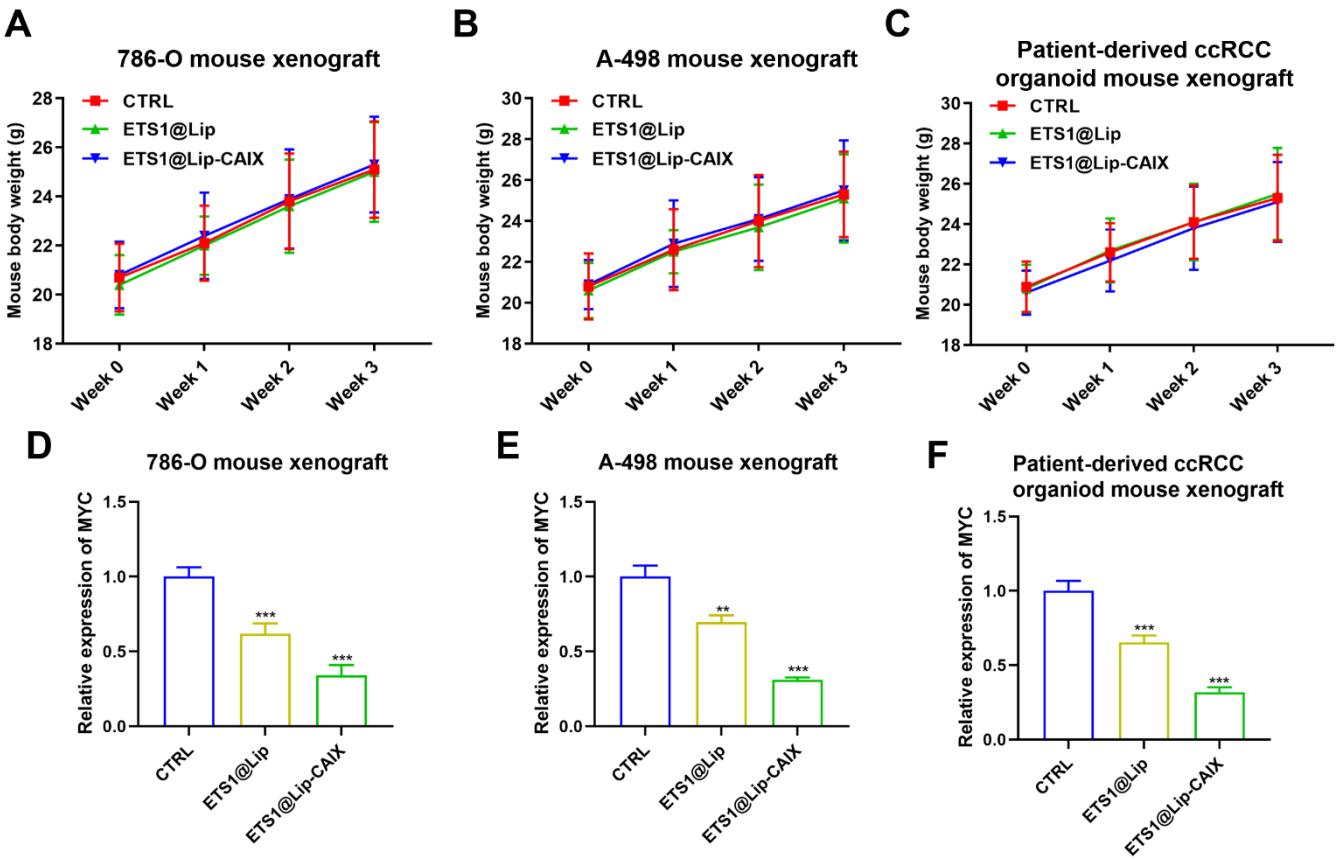


**Supplementary Figure 7 The mouse body weight and downregulation of MYC expression in nude mice xenograft models.**

(A-C) R The mouse body weight in subcutaneous xenograft tumors derived from 786-O cells (A), A-498 cells (B), and patient-derived ccRCC organoids (C) after administration of CTRL, ETS1@Lip, or ETS1@Lip-CAIX.

(D-F) Relative mRNA expression of MYC in subcutaneous xenograft tumors derived from 786-O cells (D), A-498 cells (E), and patient-derived ccRCC organoids (F) after administration of CTRL, ETS1@Lip, or ETS1@Lip-CAIX. **: $p<0.01$, ***: $p<0.001$.

**Supplementary Table**

**Table S1** TFs ranking in the top 10

| |
|---|
| FLI1, ETS1, RUNX3, EOMES, MYC, NR3C1, SMAD5, IRF4, MYBL1, STAT1 |

**Table S2** The siRNA sequences used in this study

| | |
|---|---|
| **siETS1-1 Sense** | GCAUAGAGAGCUACAUAGUTT |
| **siETS1-1 Anti-sense** | ACUAUGUAGCUCUCUAUGCTT |
| **siETS1-2 Sense** | CCAGCAUAUCAUAGACAAGTT |
| **siETS1-2 Anti-sense** | CUUGUCUAUGAUAUGCUGGTT |
| **siMYC-1 Sense** | CGAUGUUGUUUCUGUGGTT |
| **siMYC-1 Anti-sense** | ACCACAGAAAACAACAUCGT |
| **siMYC-2 Sense** | GGAACUAUGACCUCGACUAdTdT |
| **siMYC-2 Anti-sense** | UAGUCGAGGUCAUAGUUCCdTdT |
| **siCA9-1 Sense** | GACAAAGCCUGCAAGAAUUTT |
| **siCA9-1 Anti-sense** | AAUUCUUGCAGGCUUUGUCTT |
| **siCA9-2 Sense** | CCGAGCGACUUGCCUUCUUTT |
| **siCA9-2 Anti-sense** | AAGAAGGCNAGUCGCUCGGTT |
| **Scrambled siRNA Sense** | UUCUCCGAACGUGUCACGUTT |
| **Scrambled siRNA Anti-sense** | ACGUGACACGUUCGGAGAATT |

**Table S3** The primer sequences used in this study

| | | |
|---|---|---|
| **ETS1** | Forward | GATAGTTGTGATCGCCTCGG |
| | Reverse | TGCCACATTGAAAAGCACTGG |
| **CA9** | Forward | CCGAGCGACUUGCCUUCUU |

| | | |
|---|---|---|
| | Reverse | AAGAAGGCNAGUCGCUCGG |
| **MYC** | Forward | GGCTCCTGGCAAAAGGTCA |
| | Reverse | CTGCGTAGTTGTGCTGATGT |
| **CCND2** | Forward | ACCTTGGATTGCCTTTGTGC |
| | Reverse | GTTTGCCATGTTTACCAGGC |
| **CCNE1** | Forward | AAGGAGGGTGCAGCTTTTCT |
| | Reverse | CCCTGACTCCTTGACAAGGT |
| **CCD25A** | Forward | GGCCTCTTGAGTCCCCAAAT |
| | Reverse | GTAGGGAAGGACTCCAGGGT |
| **P1** | Forward | TGAGAAATTGGGAACTCCGT |
| | Reverse | TCATGTATTATGCATTATGTAT |
| **P2** | Forward | TGCACTTTCACTAGTATTCAG |
| | Reverse | TCCTCTTTCCCCTTTTATTATT |
| **P3** | Forward | ATGATCTCTGCTGCCAGTAGA |
| | Reverse | AGCTTTAAGGATTGCAAATTA |
| **P4** | Forward | TCCATAGGGTGATGTTCATTA |
| | Reverse | AGCGTCCGAGGTGCAAGGT |

**Table S4** PDI of the general LNP base formulations, the nucleic acid encapsulation efficiency and the peptide conjugation efficiency

| | **PDI** | **EE (100%)** | **peptide conjugation efficiency** |
|---|---|---|---|
| ETS1@Lip | 0.128 | 95.4 | - |
| ETS1@Lip-CAIX | 0.146 | 89.1 | 72.4% |